Non-equilibrium phase behaviour of rod-like viruses under shear flow

2004 J. Phys.: Condens. Matter 16 S3929

(http://iopscience.iop.org/0953-8984/16/38/011)

INSTITUTE OF PHYSICS PUBLISHING JOURNAL OF PHYSICS: CONDENSED MATTER

J. Phys.: Condens. Matter **16** (2004) S3929–S3939 PII: S0953-8984(04)79970-1

Non-equilibrium phase behaviour of rod-like viruses under shear flow

M P Lettinga and J K G Dhont

IFF, Institut Weiche Materie, Forschungszentrum Jülich, D-52425 Jülich, Germany

E-mail: p.lettinga@fz-juelich.de

Received 27 April 2004
Published 10 September 2004
Online at stacks.iop.org/JPhysCM/16/S3929
doi:10.1088/0953-8984/16/38/011

Abstract

We present the non-equilibrium phase diagram of rod-like colloids (*fd*-viruses) under shear flow. The shear-induced displacement of the isotropic–nematic binodal is obtained from time resolved rheology measurements. Vorticity banding is observed within the biphasic region, as bounded by the binodal. Here, in the stationary state, regular, millimetre sized bands with mutually differing orientational order are stacked along the vorticity direction. For the fully nematic phase we determine the location of transition lines from tumbling to either wagging or flow aligning, depending on the concentration. The location of these dynamical transition lines agree with theory for hard rods, when scaling to the orientational order parameter in equilibrium.

1. Introduction

Dispersions of rods are sensitive to external fields such as shear flow or a magnetic field, since they can undergo transitions in orientational order. On increasing the concentration, a first-order transition occurs, from an disordered isotropic state to an orientationally ordered nematic state. The binodal concentrations for this isotropic–nematic phase transition are fully determined by the balance between orientational and translational entropy when only excluded volume interactions are involved. When rods are subjected to shear flow, the rod orientation will be affected, so the concentration at which the transition occurs will be shear rate dependent. In other words, the location of the binodal will change on applying shear flow. The transition will cease to occur at sufficiently high shear rates where shear aligning forces dominate over inter-rod forces. The binodal thus closes on itself in the shear rate versus concentration plane.

At finite shear rates, banded structures of macroscopic size can be formed. There are two such structures to be distinguished: vorticity banded and gradient banded structures. In the former case, a regular alternating banded structure extends along the vorticity direction, where the orientational order in the two kinds of bands is different. The latter type of

banding consists of coexisting regions (the bands) with different shear rates extending along the gradient direction [1–3]. For rigid hard rods, gradient banding is predicted to occur in a very limited region close to the non-equilibrium critical point in the shear rate versus concentration plane [1, 4].

In addition, in the fully nematic state, stationary shear flow can induce oscillatory motion of the nematic director. That is, the shear aligned state becomes unstable in some regions in the shear rate versus concentration diagram. The trajectory which is described by the tip of the director is very sensitive to the applied shear rate and the rod concentration. At low shear rates the director undergoes a continuous tumbling motion in the plane defined by the flow and the gradient of the flow, while at high shear rates the rods align with the flow [5, 6]. At intermediate shear rates multiple solutions to the Doi–Edwards equation are obtained, which are sensitive to the initial orientation of the director [7, 8]. In a small region of the phase diagram even chaotic behaviour of the stress is found. A full theoretical phase diagram of this dynamic behaviour is presented in the contribution of Hess and Kröger in this Special Issue [9].

Experimental indications of the instabilities mentioned above have been found in various kinds of systems. Wormlike micelles at low concentrations show shear-induced phase transitions and structure formation [3, 2, 10], whereas at higher concentrations tumbling behaviour was found [11]. Also hydroxypropylcellulose, which is a liquid crystalline polymer, undergoes shear-induced phase transitions [12] at low concentrations and shows a tumbling behaviour at high concentrations [13]. Evidence for the transition from tumbling to wagging has been found by Mewis *et al* [14] and Grosso *et al* [15], using nematic solutions of poly-benzyl glutamate, another liquid crystalline polymer. Direct comparison of these experiments with theory for hard rod suspensions, however, is not straightforward. In the case of polymeric liquid crystals the analysis is hampered by the fact that the inter-domain stress dominates the response at higher concentrations [16]. For wormlike micelles comparison between theory and experiment is complicated by shear-dependent scission–association kinetics [17]. To gain fundamental understanding of the above-mentioned phenomena, the ideal system would be a system of monodisperse hard rods with a very large aspect ratio (say $L/D > 100$, where L is the length and D is the thickness of the rod). For such rods, Onsager showed that in the absence of shear flow the isotropic–nematic transition concentrations can be calculated exactly on the basis of a second-virial-coefficient approach [18]. One of the few systems available that comes close to the ideal system is that of *fd*-virus suspensions. The *fd*-virus is a rod-like virus, inherently monodisperse, very thin and relatively stiff. Its equilibrium behaviour can be quantitatively predicted, taking into account the semi-flexible nature of the rods and their charge [19]. Furthermore, as will become clear in the present paper, contributions to the stress from domain boundaries are relatively small, so theoretical predictions that apply for homogeneous dispersions of rods can be employed. Moreover, we already successfully used this system to determine the average isotropic–nematic spinodal [20].

In this paper we will therefore use *fd*-virus dispersions in shear flow to access the above-mentioned shear-induced instabilities. The goal is then to determine the full non-equilibrium phase diagram (in the shear rate versus concentration plane) and show the connection between the different regions. For the director instability diagram we will discuss a direct comparison with the theory of hard rods. For the determination of the non-equilibrium binodal and the shear banding regime we added polymer to the dispersion in order to induce some attraction between the rods. This causes the biphasic region to widen, such that it is easier to access the concentration dependence of the binodal and to enhance the phase separation kinetics. We use rheology to determine the location of the paranematic–nematic binodal of sheared suspensions. We perform *in situ* macroscopic and microscopic birefringence measurements to study vorticity shear band formation. Rheology and *in situ* microscopy are used to study

the director instabilities in the fully nematic phase. In the discussion we summarize the results and suggest a connection between the different phenomena.

2. Experimental details

The viscosity and stress response was measured using an ARES strain controlled rheometer (Rheometric Scientific, Piscataway, NJ). A double-Couette geometry was used because of the fairly low viscosity of the samples under study. Microscopy under shear has been carried out using a Linkam plate–plate shear cell and a standard polarizing microscope. We used a home-built shear cell with a Couette geometry of optical glass in order to monitor the birefringence of the sheared sample. The inner cylinder has a radius of 21.5 mm; the gap width is 2.47 mm. A periscope was inserted into the inner cylinder which guides polarized light through one gap only. Transmitted light was detected through a second polarizer which is used as an analyser.

The physical characteristics of the bacteriophage *fd* are: length $L = 880$ nm; diameter $D = 6.6$ nm; persistence length 2.2 μm; and the number of elementary charges per unit length is around 10 e^- nm^{-1} at pH 8.2 [21]. Also, *fd* exhibits isotropic, cholesteric and smectic phases with increasing concentration [22, 23]. The *fd* virus was prepared according to standard biological protocols found in [24], using the XL1 blue strain of *E. coli* as the host bacterium. The standard yield is ≈50 mg of *fd* per litre of infected bacteria, and virus is typically grown in 6 l batches. The virus was purified by repetitive centrifugation (108 000 g for 5 h) and finally re-dispersed in a buffer. A buffer of 20 mM tris-HCl at pH 8.2 was used for the measurements in the fully nematic phase (isotropic to nematic phase separation occurs at 11 mg ml^{-1}). The same buffer with an extra 100 mM NaCl was used for the measurements in the biphasic region, and 12 mg ml^{-1} of dextran (507 kd, Sigma-Aldrich) was added in order to widen the biphasic region [25].

3. Theory

For spatially homogeneous dispersions of rigid rods, the *orientational* probability density function, or orientational distribution function (P), is sufficient to describe the state of the system. The temporal evolution of the orientational distribution function in shear flow can be found by solving the equation of motion of the orientational distribution function, given by the N-particle Smoluchowski equation [1, 5, 26]

$$\frac{\partial P(\hat{\mathbf{u}},t)}{\partial t} = D_{\mathrm{r}}\hat{\mathcal{R}}\cdot\left\{\hat{\mathcal{R}}P(\hat{\mathbf{u}},t) + DL^2\bar{\rho}P(\hat{\mathbf{u}},t)\hat{\mathcal{R}}\oint \mathrm{d}\hat{\mathbf{u}}'\,P(\hat{\mathbf{u}}',t)|\hat{\mathbf{u}}'\times\mathbf{u}|\right\} - \hat{\mathcal{R}}\cdot P(\hat{\mathbf{u}},t)\hat{\mathbf{u}}\times(\boldsymbol{\Gamma}\cdot\hat{\mathbf{u}}). \tag{1}$$

Here $\mathcal{R}(\cdots) = \hat{\mathbf{u}}\times\nabla_{\hat{\mathbf{u}}}(\cdots)$ is the rotation operator with respect to the orientation $\hat{\mathbf{u}}$ of a uniaxial rod, $\bar{\rho}$ is the number density of rods, D is the thickness and L is the length of the rods. Furthermore, $\boldsymbol{\Gamma} = \dot{\gamma}\hat{\boldsymbol{\Gamma}}$ is the velocity gradient tensor and $\dot{\gamma}$ the shear rate:

$$\hat{\boldsymbol{\Gamma}} = \begin{pmatrix} 0 & 1 & 0 \\ 0 & 0 & 0 \\ 0 & 0 & 0 \end{pmatrix}, \tag{2}$$

complying with a flow in the x-direction with its gradient in the y-direction.

In the absence of flow, equation (1) reproduces Onsager's thermodynamic approach for very long and thin hard rods. In the presence of shear flow, new phenomena are predicted by equation (1) in addition to the paranematic–nematic phase transition. Marrucci and Maffettone [5] were the first to solve the equation of motion for the orientational distribution

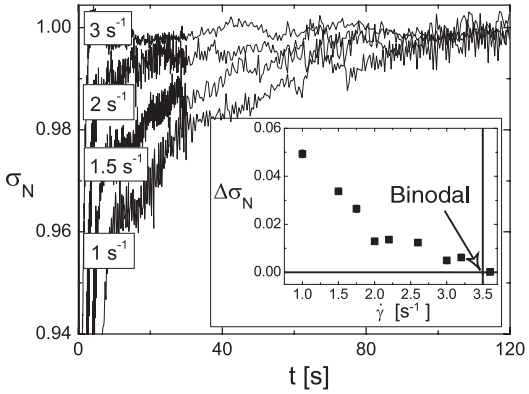

Figure 1. Determination of the binodal for $[fd] = 20$ mg ml^{-1} and $[dextran] = 12.5$ mg ml^{-1}, using shear rate quenches from the fully nematic state to the biphasic region and measuring the normalized stress $\sigma_N(t) = \sigma(t)/\sigma(t \to \infty)$. The initial shear rate was $\dot{\gamma} = 7$ s^{-1} and the low shear rates were varied between $\dot{\gamma} = 1.0$ s^{-1} (bottom) and $\dot{\gamma} = 3$ s^{-1} (top). The inset shows the magnitude of the stress response $\Delta\sigma_N$, obtained from the fit to $\sigma_N = 1 - \Delta\sigma_N e^{-t/\tau}$, as a function of the shear rate.

function numerically, restricting consideration to two dimensions in order to reduce the computational effort. They found that the director undergoes a tumbling motion with respect to the flow direction, resulting in a negative normal stress N_1. Larson used a more general solution, relying on an approximation for the excluded volume interaction term (the last term in equation (1)), in the form of a closure relation, in order to derive from equation (1) a closed equation of motion for the orientational order parameter tensor. He predicted a transition from tumbling to wagging, where the director oscillates between two small angles at somewhat higher shear rates, and finally to flow aligning at high shear rates. The use of approximation for the interaction contribution, however, can greatly bias the results, as has been discussed by Feng *et al* [27]. The location of the transitions in the shear rate versus concentration diagram is especially sensitive to the approximation, and in fact no satisfactory approximation has been found previously. In this paper we will use a finite element method to numerically solve the full equation of motion (1) for the orientational distribution function, without any approximation.

4. The non-equilibrium binodal

During the isotropic–nematic phase separation, ellipsoidal droplets (tactoids) of one phase dispersed in a background of the other phase exist. When shear is applied to the system, the tactoids will be distorted and long stripes along the flow will be formed (see the left micrograph in figure 2) and the rods in the paranematic phase will gain some ordering due to flow alignment. When approaching the binodal we observed that the contrast between the elongated tactoids and the background phase disappears, with the result that light scattering and microscopy are not useful tools for obtaining the position of the binodal. The viscosity of a rod dispersion, on the other hand, is very sensitive to ordering in the system, which makes rheology a more suitable tool for obtaining the binodal point: an increase in the viscosity is expected when a system which is forced into the fully nematic phase by applying a high shear rate is quenched into the biphasic region through a sufficient reduction of the shear rate. In figure 1 we show an example of such an experiment, where we plot the normalized stress $\sigma_N(t) = \sigma(t)/\sigma(t \to \infty)$ as a function of time after the shear rate is quenched. The initial shear rate was 7 s^{-1}, while the

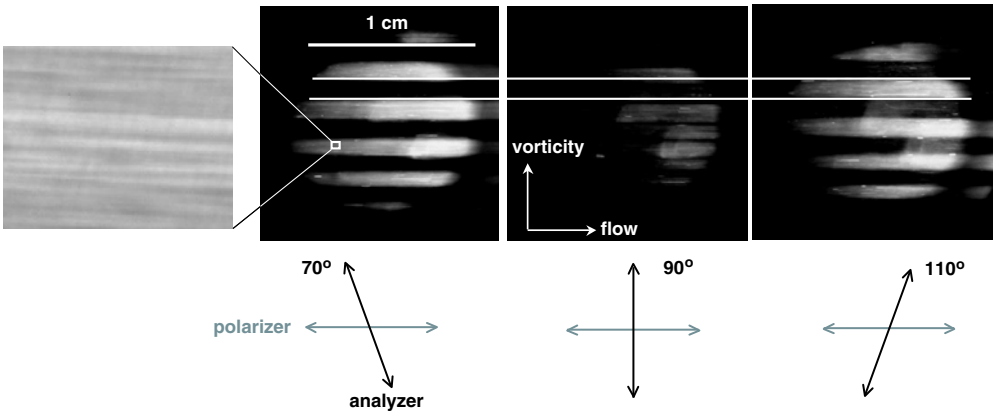

Figure 2. Three images of shear bands stacked in the vorticity direction. The images are taken by using a 1 cm radius polarized light source placed in the centre of the Couette shear cell. The analyser is placed at the other side of the gap under 70°, 90° and 110° respectively. Also shown is a close-up taken with a home-made polarization microscope within the bands, showing typical elongated regions of nematic and paranematic phases as discussed above. The shear bands are about 1 mm in height. The typical height of the elongated regions within the bands is about 10–20 μm.

(This figure is in colour only in the electronic version)

final shear rate is varied between 1.5 and 3 s^{-1}. We fitted the response to a single exponential ($\sigma_N = 1 - \Delta\sigma_N e^{-t/\tau}$), disregarding the initial fast response, which is probably due to relaxation of the pure nematic phase. The viscosity increases with a typical exponential time constant of around $\tau = 15$ s. The magnitude of the exponent $\Delta\sigma_N$ is set by the amount that the ordering in the nucleated paranematic tactoids deviates from the ordering in the nematic phase. Since the ordering in the paranematic phase increases with shear rate, it will approach the ordering of the nematic phase at the binodal. Thus $\Delta\sigma_N$ will vanish at the binodal, as can be seen in the inset in figure 1. The full binodal is found from such experiments for various concentrations obtained by mixing coexisting equilibrium isotropic and nematic phases at different ratios. The binodal is plotted in figure 3. Note that the position of the binodal very much depends on the amount of polymer added to the system. Preliminary investigations show that position of the binodal shifts to higher shear rates with increasing polymer content.

5. Vorticity shear banding within the biphasic region

In order to study the birefringence of the sheared biphasic system, we arranged a polarizer and analyser in such a way that the birefringence throughout a single gap was detected. Doing so, we observed, in addition to the formation of tactoids after a shear rate quench, the formation of macroscopic bands. The bands are stacked in the vorticity direction, indicative of an instability in that direction. The bands are up to a millimetre in height (see figure 2) and form in about 12 h. Both the size of the bands and the timescale on which they are formed are orders of magnitude larger than those for the microscopic phase separation—that is, the formation of tactoids.

Interestingly, as can be seen in figure 2, the typical biphasic structure is maintained inside the bands, and also no concentration differences are observed between the bands (data not shown). The contrast between the bands is fully determined by the differences in the orientational order. Keeping the polarizer fixed along the flow direction, the intensity of the bands can be inverted by changing the orientation of the analyser. When the angle is less than

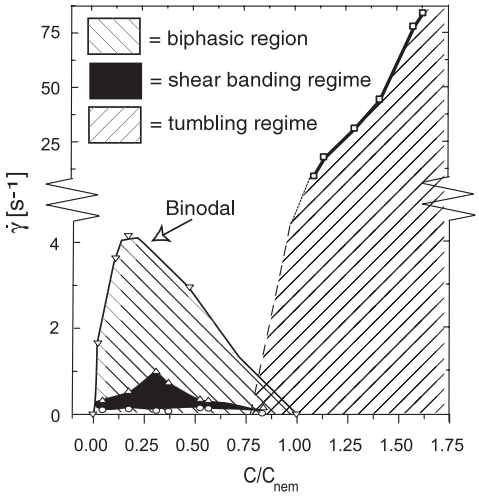

Figure 3. The experimental phase diagram of the *fd*-virus under shear. The negative hatched region indicates the biphasic region. Here the sample also contains polymer (dextran), in order to widen the concentration difference of the two coexisting phases. The black region indicates the region where the sample exhibits shear banding, which is completely contained within the two-phase region. The positive hatched region is the region where the director of the nematic phase tumbles with respect to the shear flow. The boundary given by the solid line is the experimental points in the fully nematic phase; the dashed line indicates that in the biphasic region tumbling already takes place.

90°, one band will light up; when it is more than 90°, the other band will light up. Changing the orientation of both the polarizer and analyser with respect to the shear flow while keeping them crossed does not cause a change of the relative intensity of the bands. The intensity will just increase to reach a maximum at 45° with the shear flow. Combining the two observations, it can be concluded that the polarized light is not retarded within the bands, but rotated. This means that the average orientation of the rods is tilting towards or from the vorticity direction depending on the band. This is similar to what is happening in the cholesteric phase; however, in this case the tilt is occurring in the presence of the biphasic structure.

The region in the phase diagram where the bands are formed (the black region in figure 3) is limited to the biphasic region. On the low concentration side, banding abruptly ceases to occur on crossing the binodal. On the high concentration side, banding ceases to occur at a concentration where the sample contains about 70% of nematic phase. Interestingly, at these concentrations oscillations in the viscosity after a step down of the shear rate are also observed (data not shown). As will be discussed later, these oscillations are reminiscent of instabilities in the nematic director. The concentration at which the highest shear rate is reached for which bands are still observed is somewhat higher than the concentration where the binodal peaks. The bands start to form at low but non-zero shear rates. The shear band region is fully contained within the biphasic region, defined as the region that is bounded by the binodal.

The fact that banding occurs only in the biphasic region suggests that inhomogeneities that are intrinsically present in this region are responsible for the vorticity banding instability.

6. Director dynamics in the fully nematic phase

Contrary to observations on the otherwise isotropic phase, the viscosity in the nematic phase does not monotonically shear thin, as can be seen in figure 4(a). There are two regions of shear

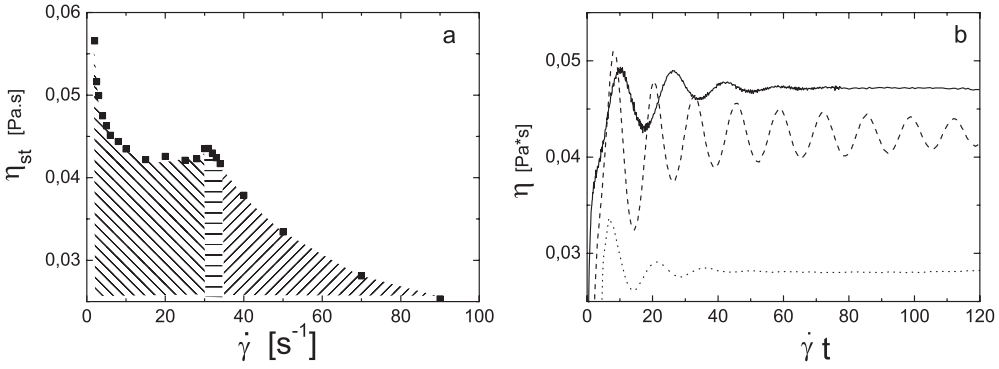

Figure 4. (a) The stationary viscosity as a function of the shear rate at an *fd*-virus concentration of 19 mg ml^{-1} or $C/C_{nem} = 1.3$. (b) The response of the viscosity to a flow reversal as a function of the strain for three different shear rates (solid curve: $\dot{\gamma} = 4\ s^{-1}$; dashed curve: $\dot{\gamma} = 33\ s^{-1}$; dotted curve: $\dot{\gamma} = 70\ s^{-1}$). The negatively hatched region in (a) corresponds to a phase where oscillations are strongly damped (solid curve in (b)); the horizontally hatched region in (a) corresponds to a phase where the oscillations are weakly damped (dashed curve in (b)); the positively hatched region in (a) corresponds to a phase of very strongly damped oscillations (dotted curve in (b)).

thinning separated by a small local maximum in the viscosity. This local maximum indicates that at this shear rate the ordering in the system is partly lost, contrary to what is expected when the degree of alignment increases with the shear rate.

In order to understand the local maximum in viscosity and to detect possible oscillatory viscoelastic responses, one needs to access the dynamic behaviour by means of transient experiments such as step down and flow reversal experiments. As mentioned in the last paragraph, the response of a pure nematic phase to a step down of the shear rate will lead to an oscillatory response of the viscosity. Likewise, an oscillatory response is seen when performing flow reversal, where the direction of the flow is suddenly reversed without changing the absolute value of the shear rate [14]. In figure 4(b) we show typical responses of the viscosity after a flow reversal for shear rates in three characteristic regions: a region where the response shows strongly damped oscillations, a region where the response is weakly damped and a region where the response is very strongly damped. Interestingly, the region of the weakly damped oscillations starts at the point where the viscosity reaches its local maximum.

This type of behaviour has been predicted by Larson, who solved the equation of motion for the orientational distribution function in an approximated way [6]. Larson argued that the nematic phase will tumble due to the torque that is exerted on those rods which have an orientation in the wings of the orientation distribution. This torque is then transmitted to the rest of the distribution due to strong excluded volume interactions between the rods. However, during the tumbling process the distribution passes the angle corresponding to the extensional direction of the velocity gradient tensor in shearing flow. At this point the distribution of the rods will be distorted with the result that the ordering will be partly lost. With increasing shear rate this effect becomes stronger and as a consequence the experimentally observed viscosity will increase. At a critical shear rate this effect is so strong that the ordering is completely lost. Since isotropically distributed rods flow align, the director will not pass the angle of extensional flow and return to the flow direction. This is the point where the so-called wagging regime is entered and where the viscosity will reach its maximum.

The damping of oscillations in the tumbling regime is probably caused by interaction between different nematic domains [28]. The explanation of the transition from strongly damped to weakly damped is then that in the wagging state the director oscillates around the

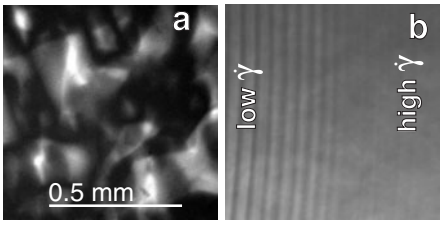

Figure 5. The structure in the nematic phase at rest (a) and at a shear rate of 250 s^{-1} (b) at a concentration of 25 mg ml^{-1}, as observed by using a shear cell with a plate–plate geometry under the polarizing microscope. Note that the shear rate increases somewhat when going from the left to the right of this picture, since a plate–plate geometry is used.

flow direction. Compared to the tumbling state, the wagging state corresponds to a more ordered state where the polydomain structure will have disappeared. This disappearance of polydomain structure at the shear rate where the viscosity reaches its maximum is demonstrated in figure 5. Here we use polarization microscopy in combination with an optical shear cell to monitor the structure. It can be clearly seen that structure disappears at a very well defined shear rate, since for a plate–plate geometry the shear rate is increasing with increasing distance from the centre. Another interesting feature shown in this image is that at this shear rate and concentration shear bands are formed. The origin of these bands, which are only formed at higher concentrations, is not clear yet and further experiments are needed. The presence of the bands does however facilitate the identification of the point where the domain structure disappears. At lower concentrations no bands are observed. Since it takes a force of 108 000 g over 5 h to sediment *fd*-virus particles over a distance of a few centimetres, which is orders of magnitude larger than the forces resulting from gradients in the shear rate, inhomogeneities as a result of shear rate gradients are negligibly small.

We can now identify the shear rate where the maximum viscosity is reached with the shear rate where the tumbling region ends and wagging sets in. Making this identification for concentrations between $C = 1.1 * C_{\mathrm{nem}}$ and $2.5 * C_{\mathrm{nem}}$ (where C_{nem} is the binodal concentration beyond which the pure nematic state is stable), we can produce a phase diagram plotting the transition shear rate as a function of concentration (■ in figure 3). In order to compare experiments with theory the shear rate and the concentration need to be expressed in dimensionless units. According to the Smoluchowski equation (1), the dimensionless shear rate, the Peclet number *Pe*, is the shear rate divided by the rotational diffusion of the rods at infinite dilution. The latter can be measured by means of electric birefringence measurements [29]. When scaling the concentration, one should consider the particles which are used not to be ideal rods, since they are somewhat flexible and charged. Therefore, the dynamic phase behaviour for ideal rods is probably *not* recovered when an experimental binodal concentration is simply scaled to Onsager's theoretical binodal concentration. It is more reasonable to compare the dependence of the transition shear rate on the orientational order parameter $P_2 = \langle \frac{1}{2}(3\cos^2(\theta) - 1)\rangle$ describing the average ordering of the rods, where θ refers to the angle between the rod and the director of the nematic phase. Since the ordering of the rods directly reflects the interaction between the rods, it is a more reliable parameter than the concentration. For *fd*-virus it was shown that order parameter was well predicted by theory, when taking the flexibility and charge of the particles into account [19]. In figure 6 we plot both comparisons of experiment and theory, rescaling the concentration to the higher binodal concentration (a) and to the order parameter in equilibrium (b). The theoretical points in figure 6 are obtained by tracking the angle between the director and the flow direction in

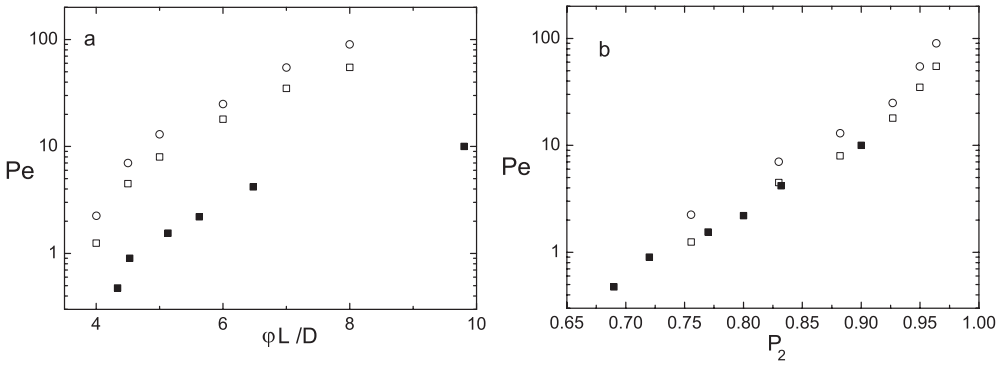

Figure 6. Comparison between the experimental and theoretical dimensionless transition shear rates *Pe* as a function of the concentration scaled to the concentration at the isotropic–nematic transition (a) and as a function of the equilibrium order parameter $P_2 = \langle \frac{1}{2}(3\cos^2(\theta)-1)\rangle$, obtained using experimental data of Purdy *et al* [19] and equation (1) for zero shear. Here θ refers to the angle of the rod with respect to the director of the nematic phase. For experiments, the tumbling–wagging transition is identified via the shear rate where the viscosity shows a local maximum (■). For theory, the tumbling–wagging transition (□) and wagging–flow aligning transition (○) are found by solving the equation of motion (1) for the orientational distribution function. The experimental shear rate is in both figures scaled to the Peclet number with the rotational diffusion at infinite dilution (21 s^{-1} [29]).

time, solving equation (1) numerically. The time dependence of this angle defines whether the system is in the tumbling, wagging or flow aligning regime.

Clearly, the scaling with respect to the order parameter gives the best comparison between experiment and theory; note that *no* adjustable parameters were used in the theory. Apparently the above-mentioned non-ideal features of the *fd*-virus are accounted for when scaling results to the same orientational order parameter. In addition, the polydomain structure of the sample, which is not included in the theory, does not seem to hamper the comparison. This is probably due to two factors. First, the viscosity of the dispersion is relatively low. It is for example about three orders of magnitude lower than that of typical polymeric liquid crystals such as PBG [16]. Second, at the transition, polydomain structure has disappeared and is therefore not important any longer. Thus, we believe that in principle all the physics is contained in the equation of motion given by equation (1). To describe vorticity banding, however, equations of motion that include spatial inhomogeneities must be derived (see [30, 31] for the derivation of such an equation).

7. Discussion and conclusion

The aim of this paper is to give an experimental overview of the phase behaviour under shear flow and the flow behaviour of rod dispersions, ranging from concentrations where the isotropic–nematic phase transition occurs up to concentrations deep into the nematic phase. A summary of the phase and flow behaviour is given in the preliminary non-equilibrium phase diagram in figure 3. As far as we know, this is the first attempt to experimentally determine a complete phase diagram under shear flow of stiff rods, ranging from low concentrations, through the biphasic region, far into the nematic region.

Measurements in the biphasic region have been performed on rod–polymer mixtures at high ionic strength, while for the pure nematic phase measurements have been performed without polymer and at low ionic strength. Comparing values for the shear rates for these two

regions as given in our phase diagram should therefore be done with caution. For example, the shear rates at which the non-equilibrium binodal is found will decrease with decreasing polymer concentration. Still missing in the experimental phase diagram is the location of spinodals for a system of attractive rods and in particular the location of the critical point. Systematic measurements to determine the full phase diagram for several polymer concentrations are in progress.

Vorticity banding is found to occur only within the two-phase region as bounded by the non-equilibrium binodal. Vorticity banding is therefore most probably the result of a normal stress related instability induced by inhomogeneities that are formed after quenching into the two-phase region. Theoretically, the challenge is to incorporate stresses that are generated by spatial inhomogeneities in orientational order (and possibly concentration) in the Navier–Stokes equation. A first attempt to derive appropriate equations of motion for stiff, long and thin rods on a microscopic level can be found in [30, 31]. Gradient banding is expected to occur close to the critical point due to critical slowing down of rotational diffusion. However, theory predicts gradient banding to occur only in a very small concentration interval near the critical point. Furthermore, theory predicts a very small difference between the shear rates in the two bands. Gradient banding of stiff rods is therefore probably very difficult to detect.

The measurements for the fully nematic phase show that the Smoluchowski theory for homogeneous rod suspensions quantitatively describes tumbling and wagging in *fd*-virus suspensions as long as the concentrations at which the transitions occur are scaled to the order parameter of the dispersion. Stresses arising from polydomains are of minor importance for these kinds of dispersions. The combination of *fd*-virus suspensions with the extension of the theory towards inhomogeneous systems is therefore promising for the full understanding of rods under shear.

Acknowledgments

We thank Zvonimir Dogic for initiating this project and for many discussions. We thank Hao Wang for the theoretical calculations. We thank Jan Vermant for the use of the rheometer and the many discussions.

References

[1] Dhont J K G 1999 A constitutive relation describing the shear-banding transition *Phys. Rev.* E **60** 4534–44
[2] Boltenhagen P, Hu Y, Matthys E F and Pine D J 1997 Observation of bulk phase separation and coexistence in a sheared micellar solution *Phys. Rev. Lett.* **79** 2359–62
[3] Lerouge S, Decruppe J P and Humbert C 1998 Shear banding in a micellar solution under transient flow *Phys. Rev. Lett.* **81** 5457–60
[4] Olmsted P D and Lu C-Y D 1999 Phase separation of rigid-rod suspensions in shear flow *Phys. Rev.* E **60** 4397–415
[5] Marrucci G and Maffettone P L 1989 Description of the liquid-crystalline phase at high shear rates *Macromolecules* **22** 4076
[6] Larson R G 1990 Arrested tumbling in shearing flows of liquid crystal polymers *Macromolecules* **23** 3983–92
[7] Faraoni V, Grosso M, Crescitelli S and Maffettone P L 1999 The rigid-rod model for nematic polymers: an analysis of the shear flow problem *J. Rheol.* **43** 829
[8] Forest M G and Wang Q 2003 Monodomain response of finite-aspect-ratio macromolecules in shear and related linear flows *Rheol. Acta* **42** 20–46
[9] Hess S and Kröger M 2004 Regular and chaotic orientational and rheological behavior of liquid crystals *J. Phys.: Condens. Matter* **16** S3835–59
[10] Britton M M and Callaghan P T 1997 Two-phase shear band structures at uniform stress *Phys. Rev. Lett.* **78** 4930–3

[11] Caputo F E, Ugaz V M, Burghardt W R and Berret J-F 2002 Transient 12 plane small-angle x-ray scattering measurements of micellar orientation in aligning and tumbling nematic surfactant solutions *J. Rheol.* **46** 927–46
[12] Grizzuti N and Maffettone P L 2003 Quiescent and flow-induced transitional behavior of hydroxypropylcellulose solutions *J. Chem. Phys.* **118** 5195–200
[13] Hongladarom K, Secakusuma V and Burghardt W R 1994 Relation between molecular orientation and rheology in lyotropic hydroxypropylcellulose solutions *J. Rheol.* **38** 1505–23
[14] Mewis J, Mortier M, Vermant J and Moldenaers P 1997 Experimental evidence for the existence of a wagging regime in polymeric liquid crystals *Macromolecules* **30** 1323–8
[15] Grosso M, Crescitelli S, Somma E, Vermant J, Moldeaers P and Maffettone P L 2003 Prediction and observation of sustained in a shear liquid crystalline polymer *Phys. Rev. Lett.* **90** 098304
[16] Walker L M, Mortier M and Moldenaers P 1996 Concentration effects on the rheology and texture of pbg/m-cresol solutions *J. Rheol.* **40** 967–81
[17] Cates M E 1987 Reptation of living polymers: dynamics of entangled polymers in the presence of reversible chain–scission reactions *Macromolecules* **20** 2289–96
[18] Onsager L 1949 The effect of shape on the interaction of colloidal particles *Ann. New York Acad. Sci.* **51** 627–59
[19] Purdy K R, Dogic Z, Fraden S, Rühm A, Lurio L and Mochrie S G J 2003 Measuring the nematic order of suspensions of colloidal fd virus by x-ray diffraction and optical birefringence *Phys. Rev.* E **67** 031708
[20] Lenstra T A J, Dogic Z and Dhont J K G 2001 Shear-induced displacement of isotropic–nematic spinodals *J. Chem. Phys.* **114** 10151–62
[21] Fraden S 1995 *Observation, Prediction, and Simulation of Phase Transitions in Complex Fluids* (*NATO-ASI Series C* vol 460) ed M Baus, L F Rull and J P Ryckaert (Dordrecht: Kluwer–Academic) pp 113–64
[22] Dogic Z and Fraden S 2000 Cholesteric phase in virus suspensions *Langmuir* **16** 7820
[23] Dogic Z and Fraden S 1997 Smectic phase in a colloidal suspension of semiflexible virus particles *Phys. Rev. Lett.* **78** 2417
[24] Sambrook J, Fritsch E F and Maniatis T 1989 *Molecular Cloning: A Laboratory Manual* 2nd edn (Cold Spring Harbor, NY: Cold Spring Harbor Laboratory Press) chapter 4
[25] Dogic Z and Fraden S 2001 Development of model colloidal liquid crystals and the kinetics of the isotropic–smectic transition *Phil. Trans. R. Soc.* A **359** 997
[26] Doi M and Edwards S F 1986 *The Theory of Polymer Dynamics* (Oxford: Oxford University Press)
[27] Feng J, Chaubal C V and Leal L G 1998 Closure approximations for the Doi theory: which to use in simulating complex flows of liquid-crystalline polymers? *J. Rheol.* **42** 1095–119
[28] Larson R G and Doi M 1991 Mesoscopic domain theory for textured liquid crystalline polymers *J. Rheol.* **35** 539–63
[29] Kramer H, Deggelmann M, Graf C, Hagenbtichle M, Johner C and Weber R 1992 Electric birefringence measurements in aqueous fd virus solutions *Macromolecules* **25** 4325–8
[30] Dhont J K G and Briels W J 2002 Stresses in inhomogeneous suspensions *J. Chem. Phys.* **117** 3992–9
[31] Dhont J K G and Briels W J 2003 Inhomogeneous suspensions of rigid rods in flow *J. Chem. Phys.* **118** 1466–78